Experimental Investigations of Hydrokinetic Turbine Providing Fillet at the Leading Edge Corner of the Runner Blades

C. Patel, V. Rathod and V. Patel[†]

Department of Mechanical Engineering, Sardar Vallabhbhai National Institute of Technology, Surat

[†]*Corresponding Author Email: vkp@med.svnit.ac.in*

ABSTRACT

Water streams with low heads can be found in India, both naturally as well as through irrigation canals. These natural resources can be used to generate electricity by utilising Hydrokinetic water turbines. The current investigation includes an experimental investigation of the axial flow turbine in order to make use of these naturally available resources. For Axial Flow Turbines (AFT), the influence of the fillet radius at the leading edge corner of the runner blade is studied. The experiments are carried out under various turbine loads and corresponding head conditions. The 3D printed runners with six different fillet radius (R_{tu}), i.e. 0 mm, 2 mm, 4 mm, 6 mm, 8 mm, and 10 mm are examined experimentally. The results are presented in the form of obtained efficiency (η) with a diverse Fillet Radius Ratio (FRR) for different Tip Speed Ratio (TSR) and equivalent head (H). The results indicate that, at the head, 0.012 m, with a sharp edge, i.e., FRR = 0 (R_{tu} = 0 mm), the minimum efficiency of 34.90% is recorded. However, at the same water head, the maximum efficiency of 84.82% is achieved with FRR = 0.046 (R_{tu} = 2 mm).

Nomenclature

R	radius of runner	Q	discharge water
R_{tu}	fillet radius at leading edge tip	Ω	angular velocity
FRR	Fillet Radius Ratio	T	torque
d_s	shaft diameter	ΔP	pressure difference
d_h	hub diameter		

1. Introduction

Hydrokinetic turbines such as Savonius, Darrieus, and Axial turbines are utilized for power production and optimized for better performance (Patel and Patel 2021). The modifications are already made for the different head Savonius as well as the Darrieus turbine in its design and by some external means (Patel and Patel 2022a). Axial turbines are increasingly being used for power generation from renewable sources, as well as for research objectives (Nunes *et al.* 2019). The low head axial turbines are easy to develop and manufacture in the remote areas where water resources are available at lower head (Quaranta *et al.* 2022). These turbines have a wide range of applications with a typical head of below 2 m globally (Fraser *et al.* 2007). The hydrokinetic turbine is divided into two categories.

The first are cross-flow turbines, while the second are axial turbines (Anyi and Kirke 2010). Hydrokinetic turbines with propellers are one type of axial turbine (Chavan *et al.* 2021). With the increased use of power propulsion in the marine area, optimised propellers are being tested on a regular basis (Higgins *et al.* 2022; Patel and Patel 2022b).

Investigations are being conducted to improve the performance of the propeller turbine. The impact of blockage and cavitation have been thoroughly investigated. (Katsuno and Dantas 2022). The axial turbines were tested for different tip speed ratios under different blockage condition (Kinsey and Dumas 2017). The major parameter which has been investigated for propeller turbines is the blade profiles. The different geometries of the blade has been studied. (Muratoglu *et al.* 2021; Du *et al.* 2022).

The winglets on the blade of an axial runner have been numerically investigated. (Barbarić *et al.* 2022). The effect of the fillet shape of the blades on the flow field has also been examined preciously. (Ananthakrishnan and Govardhan 2018; Li *et al.* 2019). Zhang *et al.* (2022) analysed the situation of a wide-chord hollow fan blade in order to improve the outcomes of the axial. According to (Tranxuan 1996), increasing the fillet reduces the stress concentration factor.

Kaplan turbines are kind of axial flow turbine that contribute significantly in the electricity generation. For the low load ratio, Kaplan turbine has high efficiency than other (Abeykoon 2022). This axial turbine performs better for the low range of head and the high discharge of water (Abeykoon and Hantsch 2017). These types of turbines are mostly investigated and adapted for the high-scale level with more than 3 meter of head (Martinez *et al.* 2019). In reality, where very low head of water is available and requirement of electricity is small, this types of axial turbine may be helpful (Maridjo *et al.* 2021). Rare study on runner blade for such a low head condition with horizontal arrangement of the turbine is found.

Based on the literature review, the effect of blockage and the designs of runner blades are thoroughly investigated. However, the detailed analysis related to the effect of runner blade edge sharpness and fillet

Fig. 1. Application of Axial flow turbine at remote location.

radius is still not investigated experimentally specifically for small head application. Hence, in the present investigation, the effect of fillet radius on the edge of leading side of runner blade is investigated in detail with different head and flow condition. The aim of the present investigation is to determine optimum size of fillet radius which provide the best efficiency. The application of axial turbine for the remote location is shown in Fig. 1.

2. CONCEPTUAL DISCUSSION ON APPLICATION OF FILLET ON LEADING EDGE CORNER

The conceptual representation of water flow striking to the turbine runner blades, specifically towards tip side is shown in Fig. 2, separately for both, turbine with sharp edges and turbine with some fillet. Figure 2(a) indicates water flow striking on the axial flow turbine runner blade with a sharp edge. Conceptually as the water strikes at the corner of the leading edge, it tries to deflect on the runner blade surface. Hence, a partial localized low pressure zone develops at the downstream side of the leading edge, which ultimately forms eddies at the downstream side with a loss of energy of water. Subsequently, the trailing edge at the downstream side of the previous runner blade passes through low energy zone of water without efficient energy conversion.

If the corner of leading edge of the runner blade is trimmed with smooth fillet as shown in Fig. 2(b), the runner blade penetrates smoothly to the upstream side water flow. It might prevent eddies formation at the downstream side of the runner blade, which leads to energy loss. Hence, the trailing edge of downstream side of preceding runner blade passes through almost streamline flow and efficiently converts hydraulic energy into, mechanical energy on runner blade. Here, it is to be noted that, excessive size of fillet radius will lead to partial flow by pass from the turbine runner blade, without conversion of energy to runner blade, which leads to fall in turbine performance. Hence, it is required to investigate the optimum size of the fillet radius, which provides the best performance from the turbine runner blade.
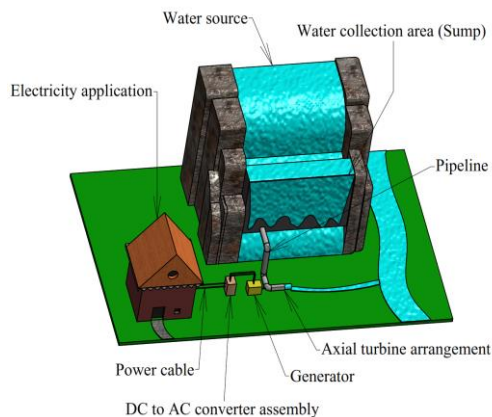

(a)   (b)
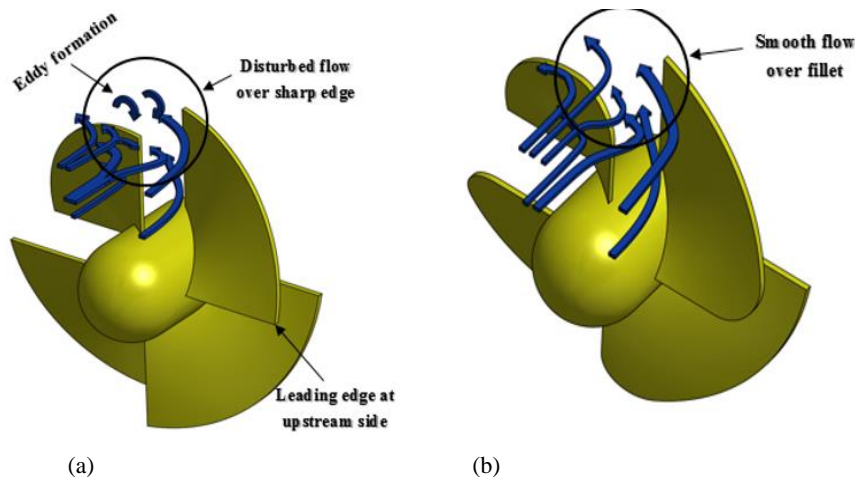
Fig. 2. Flow visualization over (a) Sharp edge (b) Curve edge.

(a) $R_{tu} = 0$ mm (b) $R_{tu} = 2$ mm (c) $R_{tu} = 4$ mm

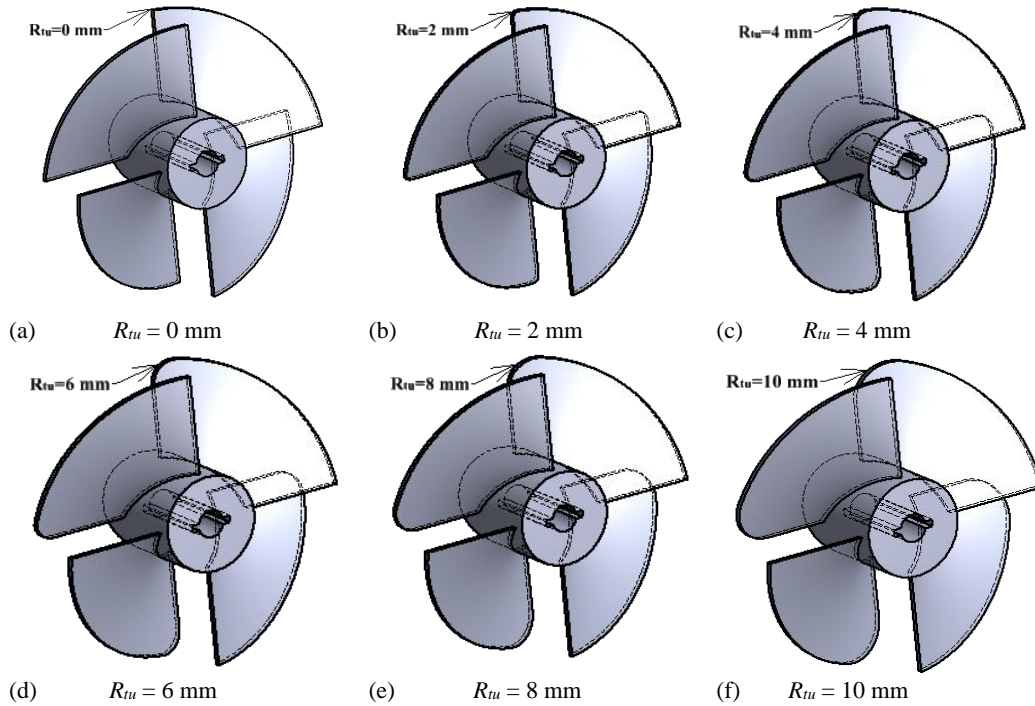(d) $R_{tu} = 6$ mm (e) $R_{tu} = 8$ mm (f) $R_{tu} = 10$ mm

Fig. 3. Investigated fillet radius at the Leading Edge Corner of the Runner Blades.

3. INVESTIGATED PARAMETERS

The aim of the present study is to improve the performance of a propeller type axial flow turbine by providing a fillet at the corner of the leading edge of the runner blade. The 3D view of all the investigated runners with the selected fillet radius is shown in Fig. 3. For clear visualization, the back side view of the runner is presented.

The six different sizes, 0 mm, 2 mm, 4 mm, 6 mm, 8 mm, and 10 mm are selected for the present investigation. All of the modified runners had the same runner diameter, hub length, and other specifications.

4. DATA REDUCTION

The terms which are frequently used in the present investigations are described as follows,

FRR (Fillet Radius Ratio) is the non-dimensional term of the fillet radius at leading edge. The ratio of the trimmed tip radius (R_{tu}) to the runner radius (R) is defined as FRR shown in Eq. (1).

$$FRR = \frac{R_{tu}}{R} \tag{1}$$

Tip Speed Ratio (TSR) is the ratio of circumferential velocity at the runner blade tip to the free stream velocity of the flow. TSR can be calculated using Eq. (2). TSR indicates the non-dimensional number of the angular velocity at the turbine runner. Indirectly it also indicates the applied load on turbine shaft/runner.

$$TSR = \frac{R\omega}{V}; \tag{2}$$

Where; runner radius (R), angular velocity of turbine shaft (ω), and water free stream velocity (V)

In the present investigation, water head on the turbine is artificially created by water pump. The head can be estimated using the pressure difference (ΔP) between the turbine's upstream and downstream sides (Yang *et al.* 2019). The equivalent head can be calculated using Eq. (3).

$$Equivalent\, Head\,(H) = \frac{\Delta P}{\rho g} \tag{3}$$

Efficiency is the ratio of mechanical power generated at turbine shaft to the energy available at turbine inlet. To compare the performance of the turbine this term has been used in the present investigation (Uchiyama *et al*. 2018). Torque (T) and angular velocity of turbine shaft (ω) are used to calculate mechanical power generation. Pressure difference and discharge (Q) can be used to calculate the amount of hydraulic energy provided to the turbine. The Efficiency can be calculated using Eq. (4).

$$\eta = \frac{\omega T}{Q\Delta P} \tag{4}$$

5. DESIGN AND MANUFACTURING OF TURBINE RUNNER

The defined dimensions are used to construct the conventional and modified turbine unit wing in 3D

modelling software. The turbine units are created using 3D printing for better dimensional accuracy.

5.1 Design

The design of turbine runner is crucial for the experimental work. The present turbine runner is designed by analysing work done by (Samora *et al.* 2016). For the better comparison, the same diameter of 101 mm for the test section is taken for the investigation. By considering the length of the turbine shaft, a clearance of about 7.5 mm has been kept in between the runner periphery and test section to make sure the runner can rotate smoothly without being in contact with the surface of test section. The runner diameter and the height is kept as 86 mm and 43 mm respectively considering the dimensions of the test section. The four numbers of blades are selected as they provide optimum performance for some cases as mentioned by (Junior *et al.* 2019). Few modifications in designs are done according to the test section available for the experiment. The detailed dimensions of the turbine is shown in Fig. 4.

For better understanding, the dimensional terms used in the present investigations are shown in Fig. 5. A few parameters are kept constant for all runners with different fillet radius.

5.2 Manufacturing of Runner

For better dimensional accuracy, the turbine runners are made using 3D printing. Initially, the conventional runner is created using the Prusha 3D printer. Figure 6 (a) shows a 3D printer used to manufacture the runner with its components. Figure 6 (b) shows the created turbine unit for the investigation.

Cura 15, a freely accessible software, was used to transform the digital part of the turbine unit design into the G-code print format. Table 1 indicates the input parameters used while creating G-codes.

To keep other parameters constant, such as surface roughness, only one unit of the runner has been manufactured. For precise marking of the fillet radius, the print of the 2D drawing of AutoCAD is used. The fillets are preciously formed using grinding machine.
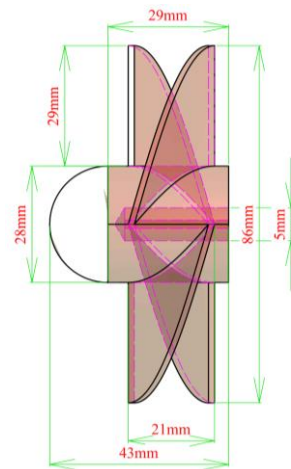

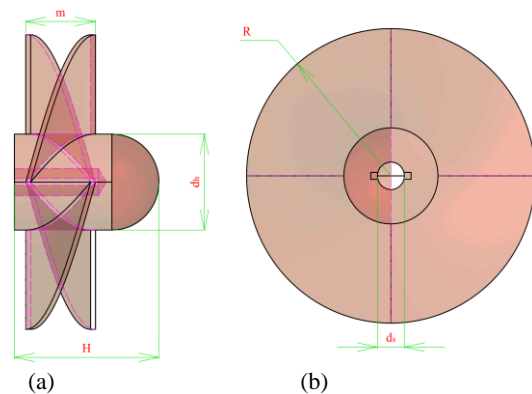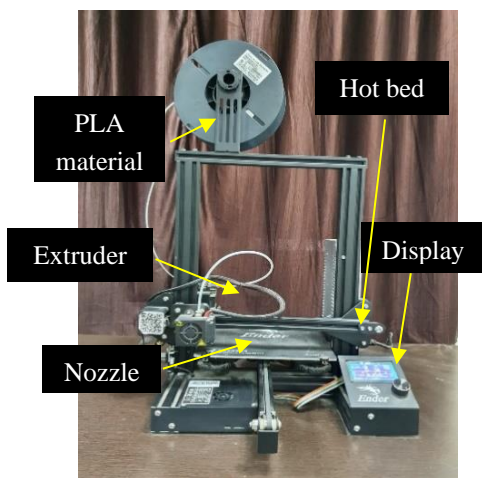**Fig. 4. Schematic diagram of conventional runner model.**

(a)   (b)

Fig. 5. (a) Side View (b) Front View of the runner drawing.

(a)   **Used 3D printer for turbine runner making.**   (b)   **Turbine unit manufactured using 3D printer.**

Fig. 6. 3D printer with manufactured turbine runner

Table 1 Input parameters used while 3D printing of turbine unit.

Parameters	Specifications
Bed temperature	60 ºC
Nozzle temperature	210 ºC
Print Speed	50 mm/s
Fill density	20%
Nozzle size	0.4 mm
Filament diameter	1.75 mm

6. EXPERIMENTAL SETUP

The various designs of turbine units are tested in the exclusive test setup. Specifically designed for testing axial flow turbines for different head conditions. The artificial head is developed using 2 Horse Power capacity of water pump. Figure 7 shows the detailed view of the developed experimental setup.

The entire setup arrangement is supported by a Mild Steel frame, as shown in Fig. 7. The construction was intended to support the load of the available pipe structure and mountings. A white PVC pipe with an internal diameter of 101 mm is used. The acrylic test section is utilised at the specific location in the pipe where turbine unit can be visible from outside. Water flows from 1000 litre capacity water tank, flow via pipe, test section and valves. Sufficiently long pipe lengths are used before turbine test sections to ensure full developed flow inlet to the turbine unit. A submersible pump has been installed inside the tank for water flow. The water flow is controlled by a ball valve installed at the downstream side of turbine unit in the pipeline. A valve also helps to control back pressure to make sure the channel is completely filled with water. The valve also used to create different pressure head condition; especially at downstream side of test section. Other flow and pressure measuring devices are used in the setup.

The arrangement of the turbine runner in the acrylic test section has been shown in Fig. 8. To visualize the flow pattern around the turbine, the transparent test section is used. The arrangement of air vent valves are also provided on the upstream and downstream sides of the test section. It is used to escape the entrapped air inside the test section before starting of the experiments. During experiments, it kept closed.
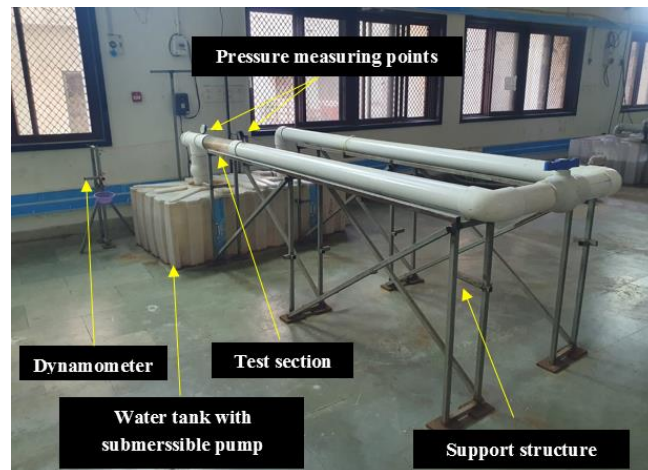

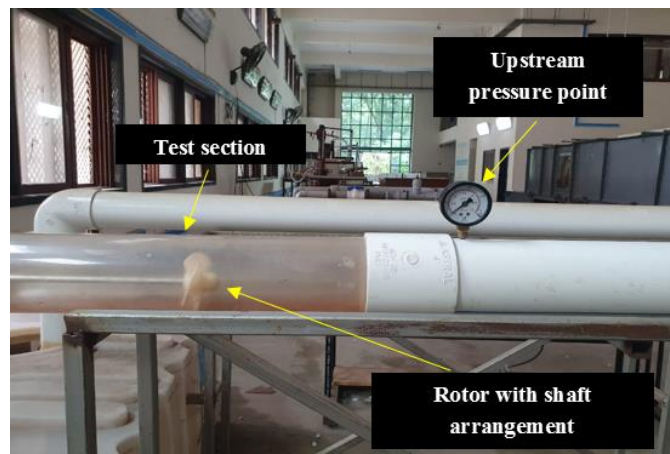**Fig. 7. Close channel experimental setup.**

Fig. 8. Turbine arrangement in test section.

The two pressure gauges are installed in the test setup. One at upstream side and other at downstream side of test section; to find the pressure difference about the turbine. The details of the test setup are shown in Table 2.

Table 2 Specifications of experimental setup.

Sr No	Details	Specifications
1	Tank Capacity	1000 Litre
2	Pump Capacity	2 Horse Power
3	Pipe Diameter	0.101 m
4	Discharge capacity of Water	2 LPS

6.1 Arrangements of Turbine Unit and Instruments in Experimental Setup

Figure 9 provides the better details of the instruments mounted on the setup and turbine shaft specifically for torque measurement. To measure the torque produced by the turbine, the rope brake dynamometer is installed. The rope is twisted around the turbine shaft to apply gradually load on the runner. Thus, the one end of the rope become tight side and the other become slack side. The tight side is connected to the externally applied load, while the slack side is connected to the spring balance to measure slack side tension. To determine the equivalent head on a turbine, the pressure difference between the upstream and downstream sides of the test section is measured using pressure gauges. To avoid bubble formation in the tank, sufficient water level is maintained inside the water collection tank and the discharge pipe is kept at sufficiently deep from the free water level.

6.2 Investigation procedure

The investigation procedure is explained stepwise as follows. Broadly, the investigation procedure is described in five major steps. (1) Design and manufacturing of the runners (2) Preparation of experiment setup (3) Arrangement of the turbine unit instruments in test section (4) Experiments on all runners with different designs (5) Results analysis.

(1) A digital model (CAD model) of 4-bladed turbine unit is prepared using solid modelling

software. The dimensions of the axial turbine runner are designed based on the available inside diameter of the test section. The G-code are generated using prepared CAD model, fill density to required strength, nozzle temperature to ensure proper melting of PLA material with the developed G-code. Manufacturing of runner is done using 3D printer.

(2) The experimental setup is prepared with the required mountings like pressure gauges, rope brake dynamometer, air vents, etc. It is required that the tank should be completely filled with water to avoid the formation of air bubbles during experiments. The air vent is used to escape the entrapped air before starting of experiments.

(3) The specific design of the turbine unit is placed in the transparent test section of the setup as shown in Fig. 10. The manufactured turbine runners used in the present investigations are shown in Fig. 11. To ensure the perfect shaft alignment, double ball bearing is used in the bearing housing of the turbine shaft. The turbine is attached to the shaft using a key and hub arrangement.

(4) The experiments on the turbine unit were carried out for all different designs of turbine units. The rope brake dynamometer is arranged at the turbine shaft for measurement of torque and variation of applied load on the turbine shaft. The angular velocity of the turbine shaft is measured using a non-contact type tachometer. The pressure difference across the

turbine is measured by pressure gauges. Each turbine unit is tested at different load conditions i.e. at different turbine speeds. Each set of parameters is tested for number of times to ensure repeatability of the results.
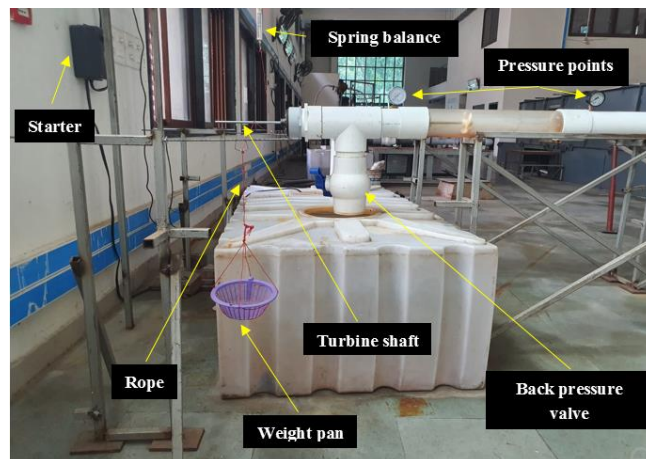

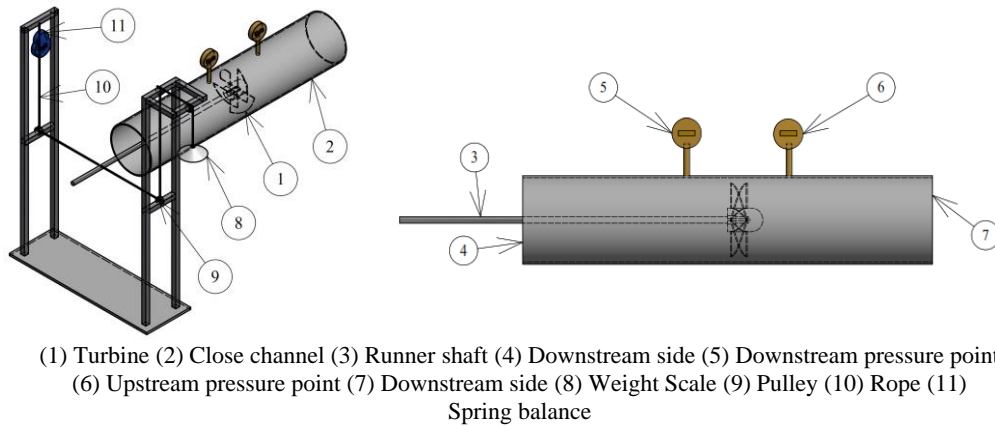**Fig. 9. Arrangement of mountings on setup.**

(1) Turbine (2) Close channel (3) Runner shaft (4) Downstream side (5) Downstream pressure point
(6) Upstream pressure point (7) Downstream side (8) Weight Scale (9) Pulley (10) Rope (11)
Spring balance
Fig. 10. Turbine arrangement in close channel

(a) FRR = 0 (R_{tu} = 0 mm)	(b) FRR= 0.046(R_{tu} = 2 mm)	(c) FRR = 0.093 (R_{tu} = 4 mm)
(d) FRR = 0.13 (R_{tu} = 6 mm)	(e) FRR = 0.18 (R_{tu} = 8 mm)	(f) FRR = 0.23 (R_{tu} = 10 mm)

Fig. 11. Modified runners for the experiments.

Table 3 Parameter conversion for various case.

Nos. of Cases	Pressure difference (Pa)	Discharge (*Q*) (LPS)	Equivalent Head (*H*) (m)	Reynolds no
Case-1	107.91	2	0.011	20,980
Case-2	117.72	1.9	0.012	20,406
Case-3	147.15	1.8	0.015	18,883
Case-4	176.58	1.7	0.018	17,833
Case-5	294.3	1.6	0.03	16,785
Case-6	323.73	1.5	0.033	15,735

(5) The obtained results are represented in form of efficiency at various TSR and equivalent head *(H)* and discharge *(Q)*. The range of these parameters are shown in the Table 3. The results are represented as Reynolds number and variable discharges. The results are presented in the non-dimensional term FRR.

7. RESULTS AND DISCUSSION

The obtained results from the experiments are presented in the form of non-dimensional term, efficiency *(η)*, Tip Speed Ratio (TSR)*,* and Equivalent head *(H)* for different FRR.
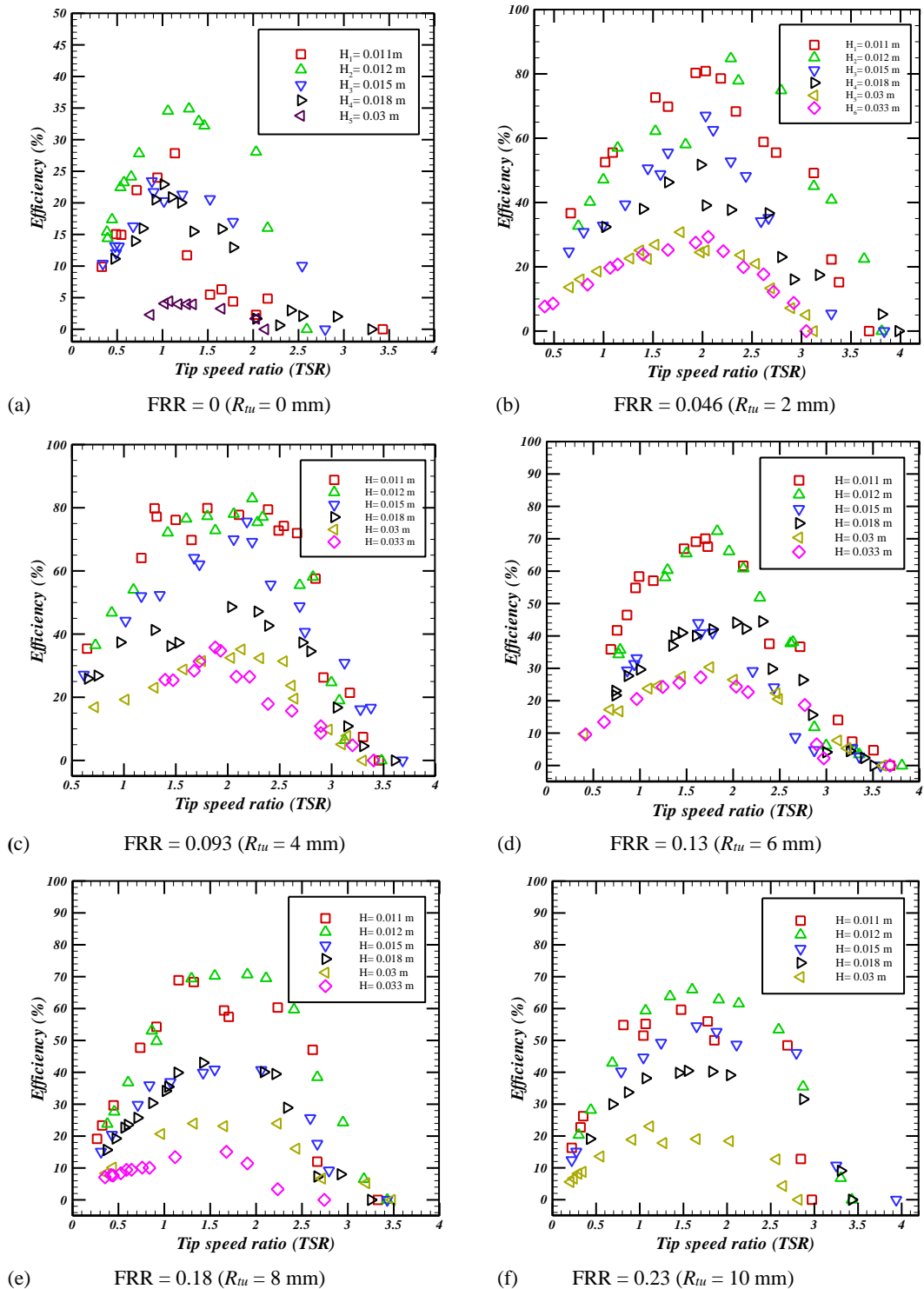
Fig. 12. Turbine performance at different applied loads with different head.

7.1 Performance of Turbine at Different TSR at Various Equivalent Head

The obtained results are presented at different TSR under various head *(H)* for each FRR separately as shown in Fig. 12. The TSR indirectly represents the load on the turbine shaft. The performance of the turbine is calculated in form of efficiency *(η)*.

The performance of the turbine with 0 mm fillet is shown in Fig. 12 (a). For specific head, initially; with application of external load, the efficiency increases and TSR falls. However after reaching to optimum efficiency value, it falls by further application of load. This pattern is observed for all different head conditions. Results also indicate that, for all investigated head conditions, maximum efficiency is observed for TSR range between 0.5 to

1.5. For sharp edge; i.e for FRR=0; the maximum efficiency of 34.90% has been measured for the 1.29 TSR at head of 0.012 m. The head 0.03 m provides lowest efficiency. The indicated maximum efficiency of 4.43% at 1.07 TSR. It is also observed that at high tip speed ratio, performance falls. This is due to the fact that; the torque generated by the turbine is typically less than the angular speed of the turbine runner. The performance of turbine at low TSR also demonstrates poor efficiency. At this region, the turbine speed predominantly falls compare to torque.

The same pattern has been observed for the remaining cases of FRR of blades. Overall, the turbine unit with FRR of 0.046 (R_{tu} = 2mm) provides the maximum efficiency of 84.82% at 2.28 TSR. However, after further increasing the fillet at the corner of leading edge side, the efficiency of the turbine decreases. This might be due to the fact that flow by pass from the fillet section may increases. The flow bypasses the turbine section without delivering its hydraulic energy to turbine runner blades. The maximum efficiency is measured as 34.90%, 84.82%, 82.93%, 72.38, 70.68% and 65.97% for FRR 0, 0.046, 0.093, 0.13, 0.18 and 0.23 at maximum TSR of 1.29, 2.28, 2.23, 1.82, 1.90 and 1.47, respectively.

From Fig. 12(a), it is also observed that the highest efficiency point at different heads for FRR=0 is falling in between TSR range of 0.5 to 1.7. Figure 12(b) indicated that the highest efficiency point; at different heads for FRR=0.046 (R_{tu} =2 mm) is falling in between 1.5 and 3 TSR. Hence, the range of higher efficiency is also enhanced by using fillet at leading edge corner. This fact indicates that by minor variation in load on turbine shaft (i.e. TSR); the rate of fall of efficiency is low for the case of fillet at leading edge corner. The same range is observed for other cases of FRR, too. This fact also indicates that fillet at leading edge corner must be utilize at the site where load on the turbine is variable, to operate it with good efficiency.

7.2 Impact of Equivalent Head and Discharge for Different Conditions

To obtain optimum head and discharge condition for selected design of turbine runner blades the variation of maximum efficiency with different head and discharge is presented in Fig. 13 for runner blades with different FRR.

For the studies, six different heads 0.011 m, 0.012 m, 0.015 m, 0.018 m, 0.03 m, and 0.033 m are reported. It is clear that 0.012 m of head produces the highest efficiency of 84.82% for FRR = 0.046. Also, the least efficiency 4.43% has been obtained for the 0.03 m head. It is also observed that for all runner blades with different FRR; with too high head the efficiency of turbine falls. This might be due to the fact that, at too high head condition the water by pass in between test sections and the turbine outer periphery. It might increase due to greater pressure difference in between upstream and downstream side. Hence, the energy due to

relatively larger head cannot be convert efficiently to the turbine runner.

Figure 13 indicates that the efficiency of all runners increases with enhancement in discharge. However, after 1.9 LPS, the results for all turbines were dropped. At 1.6 LPS, a minimum efficiency of 4.43 % reported. The runner blades with FRR=0.046, the maximum efficiency of 84.82% is achieved for 1.9 LPS.
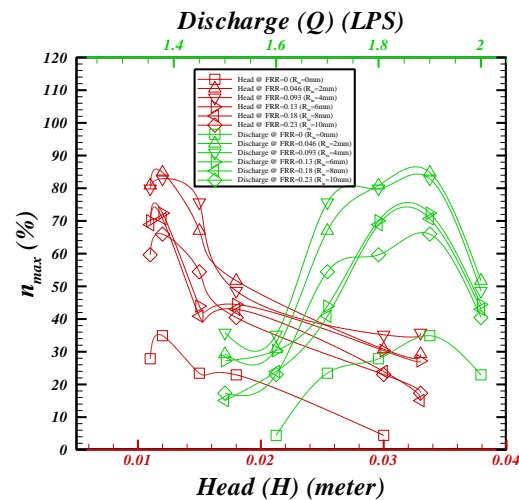

Fig. 13. Impact of head & discharge on efficiency.

It can be seen that efficiency decreases after 1.9 LPS. Overall, it is observed that the present investigated axial flow turbine provides better efficiency with high discharge and relatively smaller head of water. This is similar with the Kaplan turbine, which is also an axial flow turbine.

7.3 Performance Comparison of Investigated Fillet Radius

To conclude about optimum fillet radius, the graph of maximum efficiency obtained with different upstream side Radius Ratio (FRR) is marked as shown in Fig. 14. The maximum efficiency obtained with each fillet radius is selected for comparison. It is observed that the maximum efficiency is achieved for all cases of FRR at 0.012 m of head.

The sharp edge indicates the lowest efficiency of 34.90 % when FRR=0. The efficiency of 84.82% is observed with FRR=0.046 (R_{tu} =2 mm) at TSR of 2.28. A minor drop in performance is noted by further raising the FRR. Hence, with the present investigation, it can be concluded by using optimum fillet radius, the efficiency of turbine can be improved by 1.43% compared to sharp edges of the runner blades.

The observation has been made that the curved fillet on the corner of the leading edge produces better outcomes than the sharp edge. It is also concluded that, like the Kaplan turbine (Maridjo *et al.* 2021),
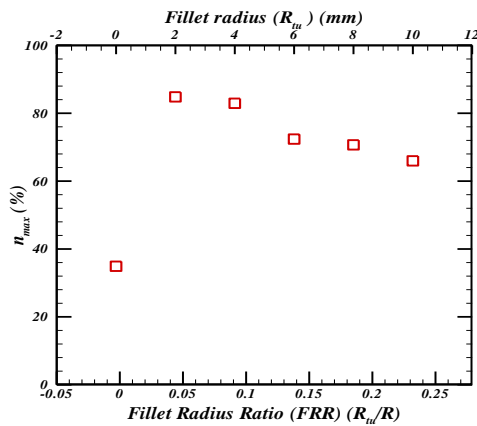
Fig. 14. Effect of fillet radius on efficiency.

the axial flow low-head turbine provides better efficiency with low-head and high flow rate conditions.

8. CONCLUSION

The objective of the present investigation is to obtain best performance of axial flow turbine by optimizing fillet at the leading edge specifically for different head applications. The experiments are carried out for six different fillet radius, i.e. $R_{tu} = 0$ mm, 2 mm, 4 mm, 6 mm, 8 mm, 10 mm (FRR= 0, 0.046, 0.093, 0.13, 0.18, 0.23). The obtained results are also indicated as a variation of efficiency with different tip speed ratio, for different vane angles and head conditions. The conclusions derived from the present investigations are marked as follows.

➢ It can be concluded that the FRR=0.046 (R_{tu} =2 mm) indicates the best efficiency of 84.82 %.

➢ The best efficiency is observed at equivalent head of 0.012 m with flow rate of 1.9 LPS for the selected design of the runner.

➢ It is observed that, the maximum efficiency of 86.70% is observed in between TSR range of 2 to 2.5. It is also observed that the values of TSR derived with FRR=0.046 (R_{tu} =2 mm) is maximum among all investigated vane fillet radius.

Appendix-I

Fillet radius (mm)	Angular velocity (ω) (rad/s)	Torque (Nm)	Head (m)	Discharge (LPS)	dη/η	Uncertainty (%)
0	10.65	0.00771	0.012	0.002	0.012	1.2
2	18.84	0.0105	0.012	0.002	0.008	0.8
4	18.43	0.0106	0.012	0.002	0.011	1.1
6	15.07	0.0113	0.012	0.002	0.009	0.9
8	15.70	0.0106	0.012	0.002	0.014	1.4
10	13.19	0.0117	0.012	0.002	0.0075	0.75

Appendix-II

Uncertainty Analysis

The uncertainty analysis has been carried out for the reported experiments results. The method for calculating uncertainty is explained as follows, The uncertainty associated while measuring these parameters is calculated using Eq. (5). Non-contact type tachometer were used to measure the angular velocity of shaft. By considering the least count associated with angular velocity *(ω)* is 0.10 rad/s. The rope brake dynamometer is used for the torque measurement. The least count associated with torque is calculated to be taken as 0.001 *Nm*. The least count for measuring the water discharge (*Q*) is 0.166 LPS. The least count in measuring the pressure difference (ΔP) is 10 Pascal.

$$\frac{d\eta}{\eta} = \sqrt{\left(\frac{dT}{T}\right)^2 + \left(\frac{d\omega}{\omega}\right)^2 + \left(\frac{d\Delta P}{P}\right)^2 + \left(\frac{dQ}{Q}\right)^2} \quad (5)$$

The maximum value of uncertainty of efficiency is 1.4 % for FRR=0.18. The concluding graph, indicating variation of maximum efficiency with different FRR, including associated error is shown in Fig. 15.
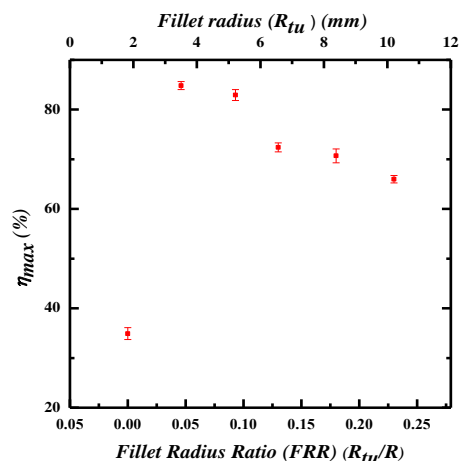

Fig. 15. Uncertainty analysis graph.

REFERENCE

Abeykoon, C. (2022). Modelling and Optimisation of a Kaplan Turbine - A Comprehensive Theoretical and CFD Study. *Cleaner Energy Systems* 3, 100017.

Abeykoon, C. and T. Hantsch (2017, June). Design and analysis of a Kaplan turbine runner wheel. In *Proceedings of the World Congress on Mechanical, Chemical, and Material Engineering*.

Ananthakrishnan, K. and M. Govardhan (2018) Influence of fillet shapes on secondary flow field in a transonic axial flow turbine stage. *Aerospace Science and Technology* 82-83, 425-437.

Anyi, M. and B. Kirke (2010). Evaluation of small axial flow hydrokinetic turbines for remote communities. *Energy for Sustainable Development* 14(2), 110-116.

Barbarić, M., I. Batistić and Z. Guzović (2022). Numerical study of the flow field around hydrokinetic turbines with winglets on the blades. *Renewable Energy* 192, 692-704.

Chavan, S. A., A. Bhattacharyya and O. P. Sha (2021). Open water performance of B-Series marine propellers in tandem configurations. *Ocean Engineering* 242, 110158.

Du, Q., L. Yunzhu, Y. Like, L. Tianyuan, Z. Di and X. Yonghui (2022). Performance prediction and design optimization of turbine blade profile with deep learning method. *Energy* 254, 124351.

Fraser, R., C. Deschênes, C. O'Neil and M.Leclerc (2007). VLH: Development of a new turbine for Very Low Head sites. *Proceeding of the 15th Waterpower* 10(157), 23-26.

Higgins, R. J., A. Zarev, R. B. Green and G. N. Barakos (2022). Investigation of a four-bladed propeller inflow at yaw. *Aerospace Science and Technology* 124, 107530.

Junior, A. C. P. B., R. C. Mendes, J. Lacroix, R. Noguera and T. F. Oliveira (2019). Hydrokinetic propeller turbines . How many blades ? *American Journal of Hydropower, Water and Environment Systems*, 2, 16-23.

Katsuno, E. T. and J. L. D. Dantas (2022). Blockage effect influence on model-scale marine propeller performance and cavitation pattern. *Applied Ocean Research* 120, 103019.

Kinsey, T. and G. Dumas (2017). Impact of channel blockage on the performance of axial and cross-flow hydrokinetic turbines. *Renewable Energy* 103, 239–254.

Li, J., X. Li, L. Ji, W. Yi and L. Zhou (2019). Use of Blended Blade and End Wall method in compressor cascades: Definition and mechanism comparisons. *Aerospace Science and Technology* 92, 738-749.

Maridjo, Slameto and Manunggal, B.P. (2021). Investigation of the utilization of kaplan turbines for pltmh power plants. *Proceedings of the 2nd International Seminar of Science and Applied Technology (ISSAT 2021)*, 207(Issat), pp. 69–73. doi:10.2991/aer.k.211106.012.

Martinez, J. J., Z. D. Deng, P. S. Titzler, J. P. Duncan, J. Lu, R. P. Mueller, C. Tian, B. A. Trumbo, M. L. Ahmann and J. F. Renholds. (2019). Hydraulic and biological characterization of a large Kaplan turbine. *Renewable Energy* 131, 240-249.

Muratoglu, A., R. Tekin and Ö. F. Ertuğrul (2021). Hydrodynamic optimization of high-performance blade sections for stall regulated hydrokinetic turbines using differential evolution algorithm. *Ocean Engineering* 220.

Nunes, M. M., C. F. M. Rafael, F. O. Taygoara, C. P. Antonio and J. Brasil (2019). An experimental study on the diffuser-enhanced propeller hydrokinetic turbines. *Renewable Energy* 133, 840-848.

Patel, R. and Patel, V. (2022a). Performance analysis of Savonius hydrokinetic turbine using 'C'shaped Deflector. Energy Sources, Part A: Recovery, *Utilization, and Environmental Effects*, 44(3), 6618-6631.

Patel, R. and V. Patel (2022b). Experimental investigation of Savonius hydrokinetic turbine with different flow diverting blocking plate. *Environmental Progress & Sustainable Energy*, 41(6), e13908.

Patel, V., S. Dixit, P. Mohit and R. Nisarg (2016). Research paper WCE2016 page experimental investigations of hydrokinetic axial flow turbine. In *Proceedings of the World Congress on Engineering,* London, U.K.

Patel, V. K. and R. S. Patel (2021). Optimization of an angle between the deflector plates and its orientation to enhance the energy efficiency of Savonius hydrokinetic turbine for dual rotor configuration. *International Journal of Green Energy* 00(00), 1-14.

Quaranta, E., B. Amir, R. Alireza and R. Roberto (2022). The very low head turbine for hydropower generation in existing hydraulic infrastructures: state of the art and future challenges. *Sustainable Energy Technologies and Assessments* 51, 101924.

Samora, I., H. Vlad, M. Cecile, J. F. Mario, J. S. Anton and M. R. Helena (2016). Experimental characterization of a five blade tubular propeller

turbine for pipe inline installation. *Renewable Energy* 95, 356-366.

Tranxuan, D. (1996). Optimum fillet radius for a latch. *Computers and Structures* 61(4), 645-650.

Uchiyama, T., S. Honda and T. Degawa (2018). Development of a propeller-type hollow micro-hydraulic turbine with excellent performance in passing foreign matter. *Renewable Energy* 126, 545-551.

Yang, W., H. Yimin, J. Huiting, L. Benqing and X. Ruofu (2019). Lift-type and drag-type hydro turbine with vertical axis for power generation from water pipelines. *Energy* 188, 116070.

Zhang, X., W. A. N. G. Yanrong, C. H. E. N. Weiyu and X. Jiang (2022). Parametric study on the flutter sensitivity of a wide-chord hollow fan blade. *Chinese Journal of Aeronautics*.